Development of time-resolved 3D-diffraction-tomography to Study Ongoing Carbonation in Concrete

A. González-Saborido[1,2], M. Tyrer[3], S.D.M.Jacques[1,2], M.Vickers[1,2] and P.Barnes[1]

[1]Materials Chemistry Centre, University College London, 20 Gordon Street, London WC1H 0AJ, UK; [2]School of Crystallography, Birkbeck College, London WC1E 7HX, UK; [3]Department of Materials, Imperial College, London SW7 2AZ, UK.

Abstract

A new synchrotron-based non-destructive X-ray tomography, termed 'Tomographic Energy Dispersive Diffraction Imaging' (*TEDDI*), has been developed and extended for application to problems associated with cementitious systems, including those involving cement carbonation. *TEDDI* is an imaging technique with the capability of non-destructively locating structural and chemical content within sizeable dense objects, such as concrete cores and cement barrier systems. It is being used in this study to follow, long term, the process of carbonation through either enhanced (sodium carbonate solution) or natural (atmospheric) causes and in particular the *TEDDI* experiment has been configured to follow carbonation at both microscopic (porous regions) and macroscopic (major fracture) levels; this involves using two levels (coarse and medium) of spatial resolution and assembling three-dimensional data sections to cover the extremities of large features. In this way *TEDDI* is providing an ongoing *in situ* space-time description of carbonation, in both model and real cement systems. One model feature is the deliberate introduction of an artificial major fracture into a concrete core so as to observe its long term influence on carbonation. The current results are presented as a series of uncorrected phase maps in 2-dimensional sections from which the distribution of identified crystalline phases can be inferred. At this point in the study no calcium carbonate phase could be identified in the *TEDDI* data, indicating that the extent of carbonation was minimal.

1 Introduction

A potentially powerful technique is being developed that will allow the interior of cement or concrete cores to be repeatedly and non-destructively examined *in situ* during exposure to conditions such as atmospheric or artificial carbonation. This technique is an extension of a synchrotron-based technique, known as *TEDDI* (Tomographic Energy Dispersive Diffraction Imaging) which had been used previously [1] to gain structural/compositional images of interior sections of bulk objects; such objects included concrete test cores [2-4] and, in particular, one of these

studies [2] revealed portlandite to calcite (CH → CČ) conversion in the outer 8-10mm of cores that had been weathered for 24 years. However these studies were limited in both the time and space domains: if such imaging techniques are to follow ongoing cement processes taking place in detail it is necessary to configure the *TEDDI* technique to a new level. This has been done in the present study whereby *TEDDI* has been used in a three-dimensional sense for the first time as part of ongoing (long term) study of cement carbonation; the 3-dimensional aspect is arrived at through configuring a *series* of two-dimensional *TEDDI* slices in which the pixel resolution can be varied from coarse (1 mm) to cover large scale (e.g. crack) features, to more fine (200 μm) to highlight regions of fine porosity. Furthermore by repeatedly re-visiting and re-imaging the same regions over a long period of time (minutes to months) *TEDDI* can build up a more detailed picture of processes such as carbonation comparing, for example, accelerated and natural carbonation and examining the roles of large scale cracks and fine pores. In this study we have initiated a long term study of concrete carbonation using this approach and in combination with traditional electron microscope and X-ray diffraction techniques.

Cement carbonation is a very appropriate topic for study by *TEDDI*, being a familiar process involved in maturation and degradation of cements exposed to the atmosphere [5,6,7]. In structural concrete, the outermost region undergoes reaction with atmospheric carbon dioxide which, through dissolution in pore moisture, is free to react with both portlandite and the calcium-rich domains in calcium silicate hydrate (CSH), to form calcite (CČ). As the molar volume of calcium carbonate is greater than that of its forming reactants, the carbonation process is largely self-limiting, as porosity is reduced at the surface through pore closure and carbonation is very much slower within the body of the core. This ideal condition is, however, occasionally not met due to the presence of preferred CO_2 transport pathways (i.e. fractures or regions of poor compaction) or corrosion of steel reinforcement. This and the relatively simple crystalline phase transformations associated with carbonation (e.g. CH + Č → CČ + H) make long term concrete carbonation an attractive system to study with the extended *TEDDI* technique outlined in this paper.

2 Materials and methods

Low aluminium and iron content (C_3A content: 4-5% by mass, C_4AF content: 1% by mass) white cement manufactured by Aalborg White ® (Aalborg Portland Group, Denmark) was supplied by Castle Cement Ltd. and stored at room temperature prior to use.

Cement pastes were prepared at water-cement ratios of 0.5 and cast into cylinders (Ø=25mm × L=75mm) with vibration to remove any entrapped air bubbles. The sealed cylinders were rotated for 36 hours at low speed (10

rpm) to minimise segregation and bleeding during setting. Subsequently the air-tight containers were stored at 25°C for 63 days. On opening, one of the samples was partially cut using a hack saw and then split vertically using a sharp chisel. The two fragments were re-assembled, but with glass wool inserted at the top and bottom to keep the two faces apart, by a few hundred microns. The re-assembled sample was wrapped in gas-tight polymer film to limit atmospheric carbonation prior to examination. Pre-carbonation experiments were carried out, and then the cylinder was unwrapped and immersed in sodium carbonate solution (0.1M *aq.*) for 2 hrs prior to the current first post-carbonation measurements. SEM samples were prepared in the same way, though choosing smaller fragments of the sample suitable for the machine, and they were later mounted on a stub and carbon coated.

PXRD data were collected using a Stoe STADI-P diffractometer equipped with a cobalt anode running at 40kV, 30 mA with a Ge-111 primary-beam monochromator and a small linear position-sensitive detector (PSD) covering approximately 5° in 2θ. Samples were prepared by crushing in a pestle and mortar, passing through a 38 μm sieve and mounting in 0.3 mm capillaries; carbonated samples were obtained from scraping a small amount of material from the surface of one of the unused carbonated SEM samples. Data were collected from 5 to 70° 2θ with 0.1° 2θ steps. The post-carbonated data were collected at 50 s *per* step but run twice to monitor consistency in diffractometer alignment. For the pre-carbonated sample, data were collected at 70 s *per* step. Binning at 4 channels *per* point gave a data step resolution of 0.02° 2θ.

2.1 *TEDDI* method

Synchrotron-based *TEDDI* (tomographic energy dispersive diffraction imaging) has been developed [1,2,8] as an imaging technique with the capability of non-destructively locating structural and chemical content within sizeable dense objects, such as concrete cores with ~centimeter dimensions, even when surrounded by supporting apparatus such as a heater. This degree of penetration is achieved through using very intense hard white X-ray beams as available on second/third generation synchrotron wiggler (magnet) devices. The technique relies on a fundamental aspect of energy-dispersive diffraction, that it is a method in which diffraction patterns are collected as intensity-energy plots, rather than intensity-angle plots as in conventional X-ray diffraction, so that the diffractometer is stationary during pattern collection; therefore by restricting the incident and diffracted X-ray beams (by use of slits and a collimator, see figure 1) one can define a small volume element, or voxel, within the sample-object from which the detected diffraction pattern derives. Then by scanning the sample across the incident X-ray beam one can arrange that this volume element visits all required regions within the sample. This scanning is performed by an *xyz* stage which

traditionally follows a 1D (line) or 2D (area section) grid. Uniquely, for this study carried out on station 16.4 [9] of the "SRS" synchrotron Radiation Source at the Daresbury Laboratory, UK, a three dimensional grid was used for the first time in order to follow processes in fine detail while also gaining coarse information about macroscopic features such as a core fracture. Furthermore by using three energy-dispersive detectors, at three different angles (see figure 1), three different versions of the diffraction pattern can be simultaneously collected, each covering a different range of crystal *d*-spacings [10]. In this particular study the "top" detector (at a collection angle of 2θ=7.576°) generally provided the most useful information. With this detector and the X-ray beam slit/collimator combinations available it was possible to select a "coarse" *TEDDI* mode with a voxel size of 8.3 mm^3 and grid step of 1 mm or a "medium" (more fine) mode with a voxel size of 0.09 mm^3 and grid step of 200 μm. Once a full *TEDDI* data set has been collected for the sample, be it over 1-, 2- or 3-dimensions, the associated bank of diffraction patterns can be interrogated for features of interest such as specific diffraction or fluorescence peaks that are representative of a given mineral phase or even mineral sub-species or crystalline polymorph. The chosen diffraction or fluorescence features can then be interpreted by assembling intensity maps showing the concentration of certain phases (from the diffraction data) or desired atomic elements (from the fluorescence data) within the sample. In this study 2- and 3-dimensional maps were assembled using major diffraction peaks to represent concentrations of unhydrated cement (C_2S), hydrated cement (CH, CSH) and carbonation (CČ), as detailed in the following figures.

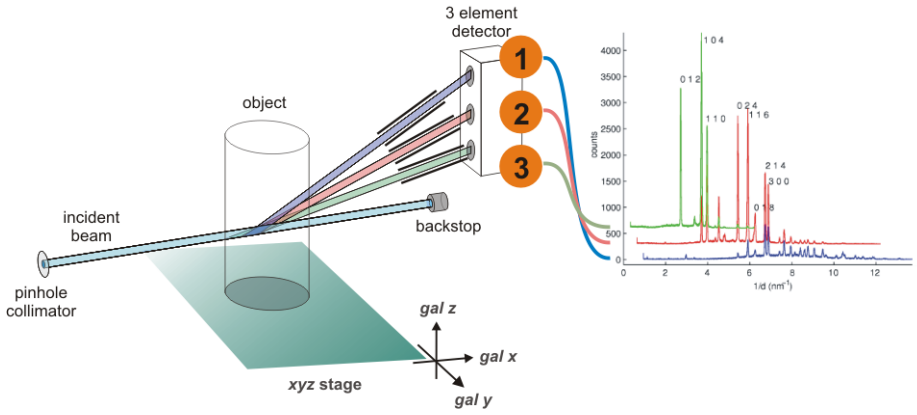

Figure 1: Schematic of the *TEDDI* set -up combined with the 3-element detector-collimator [10] system available at station 16.4 [9] of the Synchrotron Radiation Source (SRS), Daresbury. See main body of text for explanation.

2.2 Analysis method of *TEDDI*

Intensities were extracted by a whole-pattern Le Bail [11] based method using Rietica software [12,13]. The phases included in the model where C_2S, CH, CSH and CČ, details of which are given in table 1. Several low intensity reflections, from all phases, were excluded. This significantly reduced the likelihood of intensity mis-assignment.

Cement Nomenclature	Source + [reference]	Details
C_2S	ICSD: 81096 [14]	SG: P 1 2 1/N 1 a=5.5121, b=6.7575, c=9.3158, α= γ=90, β=94.581
CH	ICSD: 91882 [15]	SG: P $\bar{3}$ M 1 a=b=3.5682, c=4.8625, α=β=90, γ=120
CSH	JCPDS: 32-165 [16]	SG: P 1 a=10.59, b=7.278, c=9.53, α=101.0, β=105.8, γ=110.1
CČ	ICSD: 52151 [17]	SG: R $\bar{3}$ C H a=b=4.991, c=17.062, α=β=90, γ=120

Table 1: Phases included in the Rietica model and their details, used in the analysis of the *TEDDI* data.

3.1 SEM results

(a) (b)

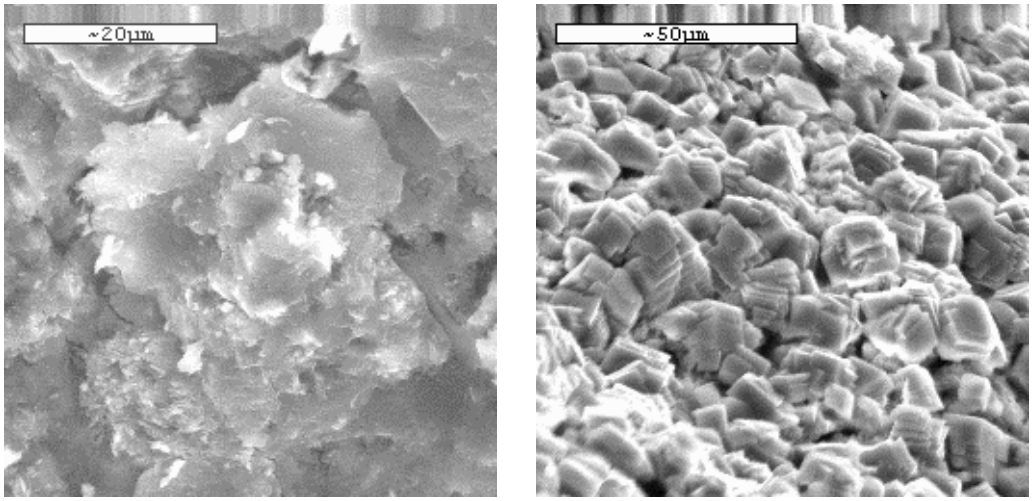

Figure 2: SEM micrographs of fractured surfaces of (a) pre- and (b) post-carbonated hydrated white cement samples; samples were carbon coated.

Two small pieces of material from the same batch than the measured core were examined by electron microscopy (JEOL Type 35-T machine) pre- and post- an accelerated carbonation event; the post-carbonated sample was left 2hrs in a rich carbonated environment (at 0.1M *aq*) in a manner similar to the fractured core under study. Figure 2 shows the electron microscope pre- and post- carbonated images. Figure 2a shows the fracture surface of a hydrated white cement paste with large CSH features in the background and broken foils of CSH in the central foreground; in the upper right is a tabular portlandite crystal. Figure 2b shows multiple tabular calcite crystals growing on the fracture surface of carbonated hydrated white cement.

3.2 XRD results

Figure 3 shows the XRD traces for pre and post carbonated samples. The pre-carbonated sample (figure 3a) gave good matches with CH and C2S. A reasonable match was also found with CSH but no positive match could be found with any CC̆ phase. The post-carbonated sample (figure 3b) gave similar matches as above but with an additional positive identification for calcite. In both cases there is a large background, greater than can be accounted for by the glass capillary alone and this is likely to be due to a non-crystalline component in the sample. Both samples are dominated by CH and by the non-crystalline component. There is also a very small amount of unidentified crystalline material characterised by two small peaks around 10° 2θ.

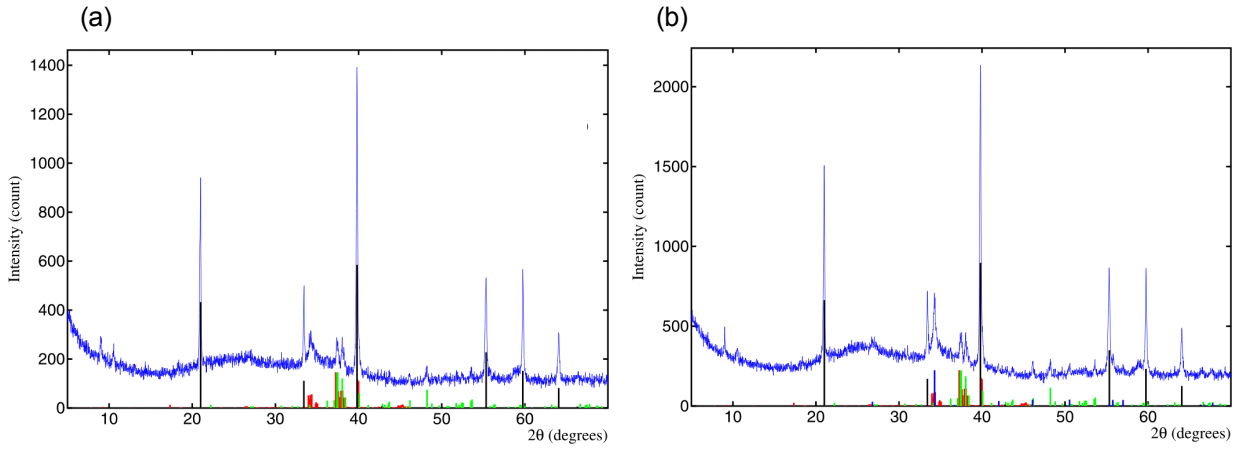

Figure 3: XRD of (a) pre- and (b) post-carbonated hydrated white cement samples. Overlaid on the XRD are stick intensities of identified phases from the ICDD database: CH (black), C2S (green), C3S (red) and CC̆ (blue).

3.3 *TEDDI* results

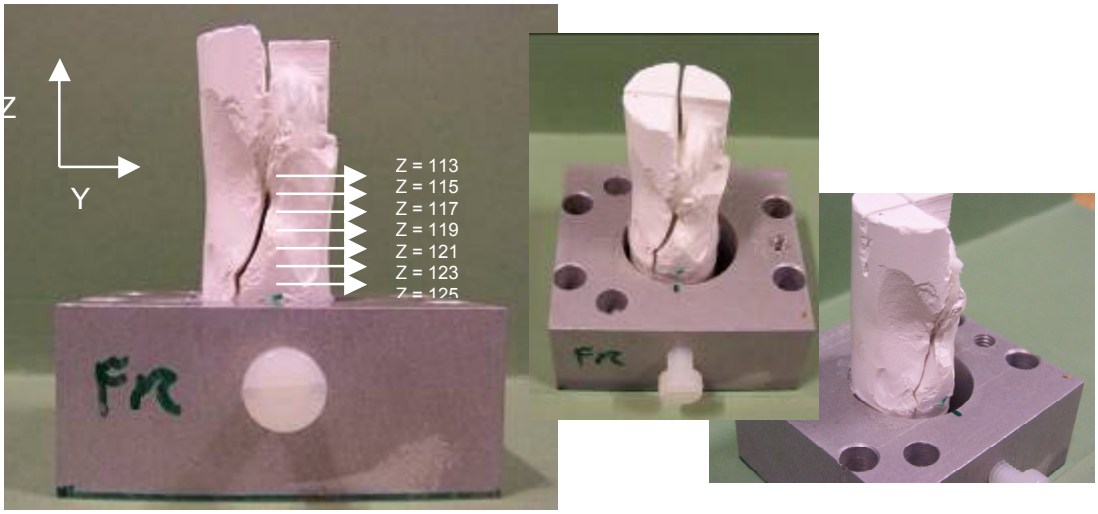

Figure 4: Front view and aerial view photographs of the fractured hydrated white cement core in its mount. The arrows on the core indicate the set of 2D traverses made along the *z* direction over a fractured region.

Figure 4 includes front and aerial view photographs of the fractured hydrated white cement core, whose preparation is described above. Overlaid on the photograph are the positions in the *z* axis (*galz* motor) where a set of coarse (1 mm resolution) 2D *xy* traverses were used (via the *galx* and *galy* motors) for pre- and post-carbonation TEDDI analysis of this core. Figure 5a shows the total diffracted intensity distribution (in the post-carbonated state) at one fixed position in *z* axis, *galz* = 113; this heat map represents the sum of each EDD spectrum recorded at each point in the *xy* traverse, where the accompanying colour-bar shows the intensity. *galx* at value 66 corresponds to the front of the core and at value 90 to the back of the core; similarly *galy* at value 101 corresponds to the left side and at value 78 corresponds to the right side (note the plot axis is reversed). The fracture can be seen running almost vertically (in the figure image) from the front of the core at *galy* = 92 towards the back of the core. There is high intensity clustering on the left and right regions of the core compared with the bulk of the sample where increased path length has resulted in greater X-ray absorption. Figures 5b – c show the distribution of the 0 1 2, 2 2 $\bar{3}$ and 6 0 $\bar{6}$ reflections, recorded at 49.1, 51.8 and 43.1 keV respectively; such maps can be generated for almost any measured reflection. The fracture is clearly visible in all plots as is the intensity clustering. The apparent distribution of C_2S seems 'more even' in the bulk of the core than is observed with the distributions of CH and CSH. However, these differences again largely result from absorption effects. Most importantly, no calcite, nor indeed any other CČ phase could be identified by *TEDDI* within the bulk core up to and including the time of the 2 hr accelerated carbonation event.

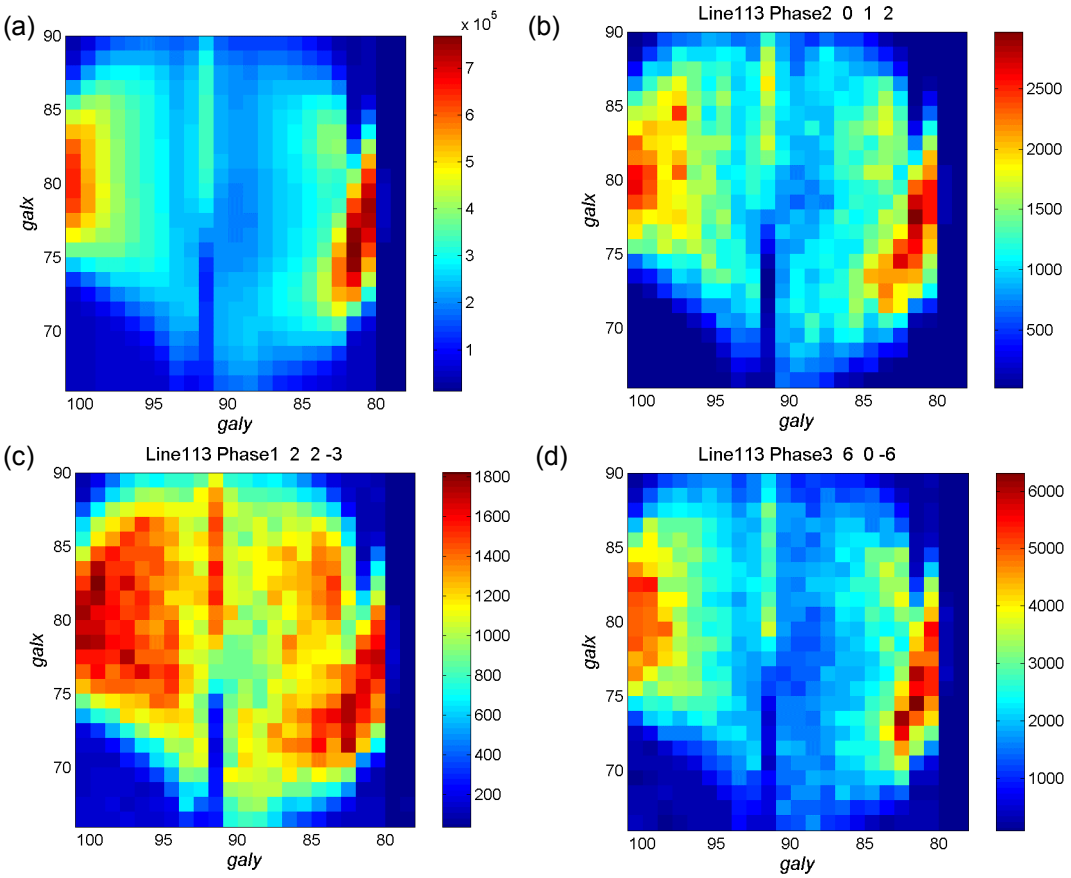

Figure 5: Intensity distribution plots of the xy (galx-galy) plane of the carbonated core at position 113 in z direction (galz motor): (a) map of total diffracted intensity, (b) portlandite 012 reflection (recorded at 49.1 keV), (c) dicalcium silicate (C_2S) 22-3 reflection(recorded at 51.8 keV), (d) CSH 60-6 recorded at 43.1 keV.

The effect is demonstrated in figure 6 where the intensity distributions for two other portlandite reflections (recorded at two other energies) are presented; these can be compared to the intensity map for the 0 1 2 reflection given in figure 5. The reflection at lower energy (36.0 keV) suffers greater X-ray attenuation than the reflection at higher energy (65.3 keV). At the moment of writing we do not have a convenient correction method for displaying absorption-corrected phase distributions for such a sample, though this is 'work in progress'; henceforth, all such figures are uncorrected in this respect, and due allowance should therefore be made in the interpretation.

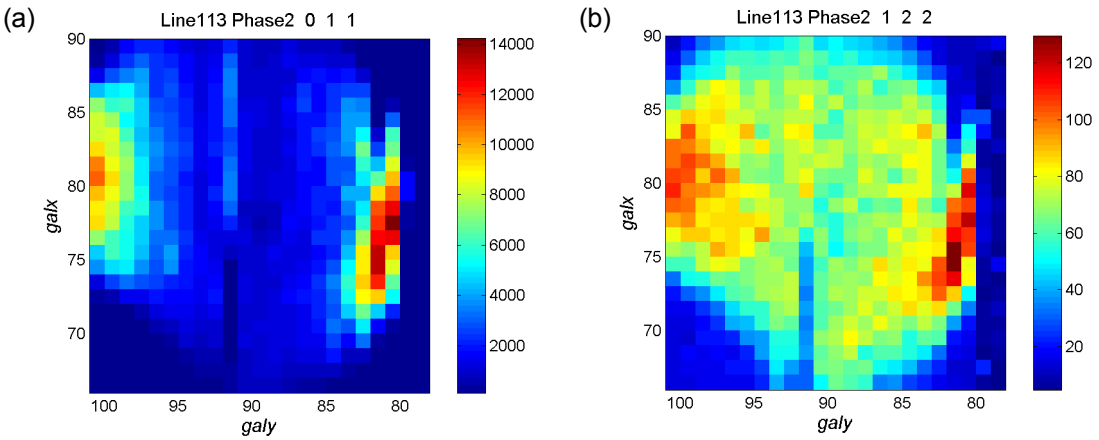

Figure 6: Intensity distribution plots of two portlandite reflections. (a) 0 1 1 and (b) 1 2 2 reflections recorded at 36.0 and 65.3 keV respectively. These plots are derived from data recorded at position galz = 113.

Figure 7 presents a set of 2D images at different positions in *galz* for a given portlandite reflection from the upper (*galz* = 113) to the lower (*galz* = 125) scanned region of the sample. The fracture progresses down the core throughout the scanned region where its position changes as a function of *z*, i.e. it is not aligned with the vertical centre axis of the core. The cross section of the core changes slightly at each position of *galz* (due to the nature of its fractured surface) and this has implications to the X-ray path length at each position in *galy*. As indicated in the legend, the first and second halves of the data shown in plot 6e were recorded pre and post a synchrotron refill and this is apparent in the sudden and obvious intensity change.

Comparison of pre- and post-carbonation data, show no significant changes in CH distribution, even upon close inspection; see figure 8. This is consistent with no significant carbonation occurring.

In addition to the coarse scan, a more space-limited but finer (200 μm resolution) scan of the fracture was made. The scanned region and results are presented in figure 9. Again, no $CaCO_3$ phase was detected. It can be seen from the intensity distributions that the main fracture proceeds vertically in the plot though taking a rightward 'kink' at *galx* = 79. The distribution also indicate a smaller fissure running from the top left of the plot and downwards, but it is difficult to confirm this without having made the necessary absorption corrections. It must be remembered that this is a visualisation within a solid object and, until the entire experiment has been completed, the sample must not in the interim be destroyed in order to confirm its structure by other techniques.

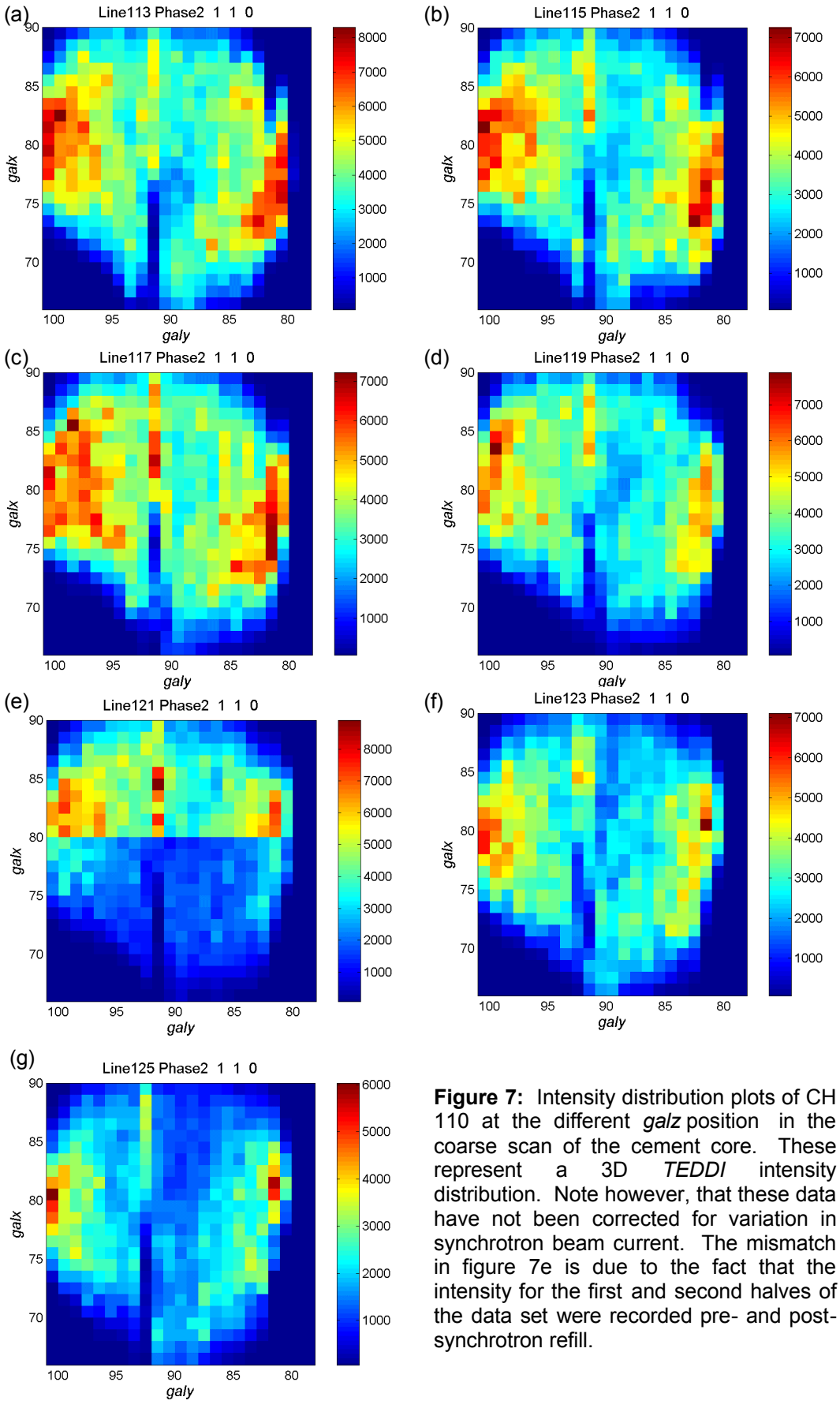

Figure 7: Intensity distribution plots of CH 110 at the different *galz* position in the coarse scan of the cement core. These represent a 3D *TEDDI* intensity distribution. Note however, that these data have not been corrected for variation in synchrotron beam current. The mismatch in figure 7e is due to the fact that the intensity for the first and second halves of the data set were recorded pre- and post-synchrotron refill.

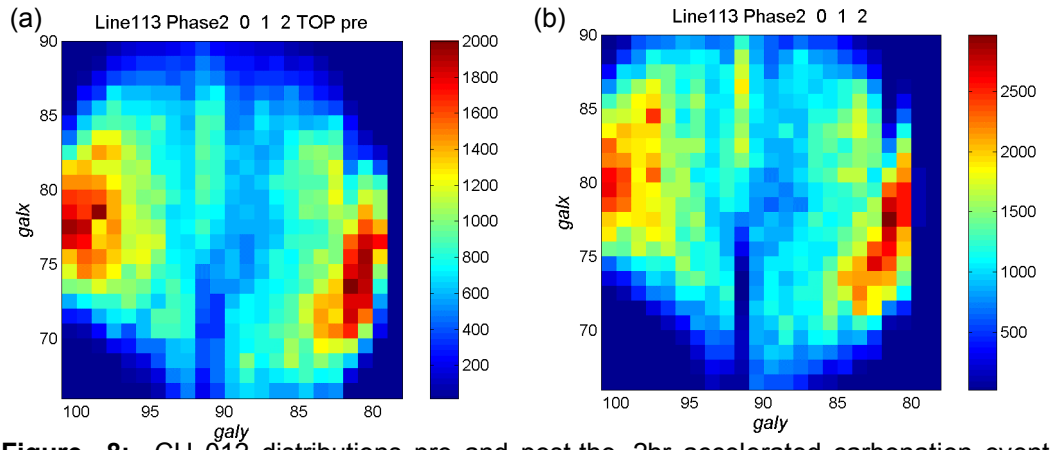

Figure 8: CH 012 distributions pre and post the 2hr accelerated carbonation event. Note that the images are slightly offset from one another due to a slight misalignment of the *xyz* stage in the post-carbonation measurements. These plots are derived from data recorded at position *galz* = 113.

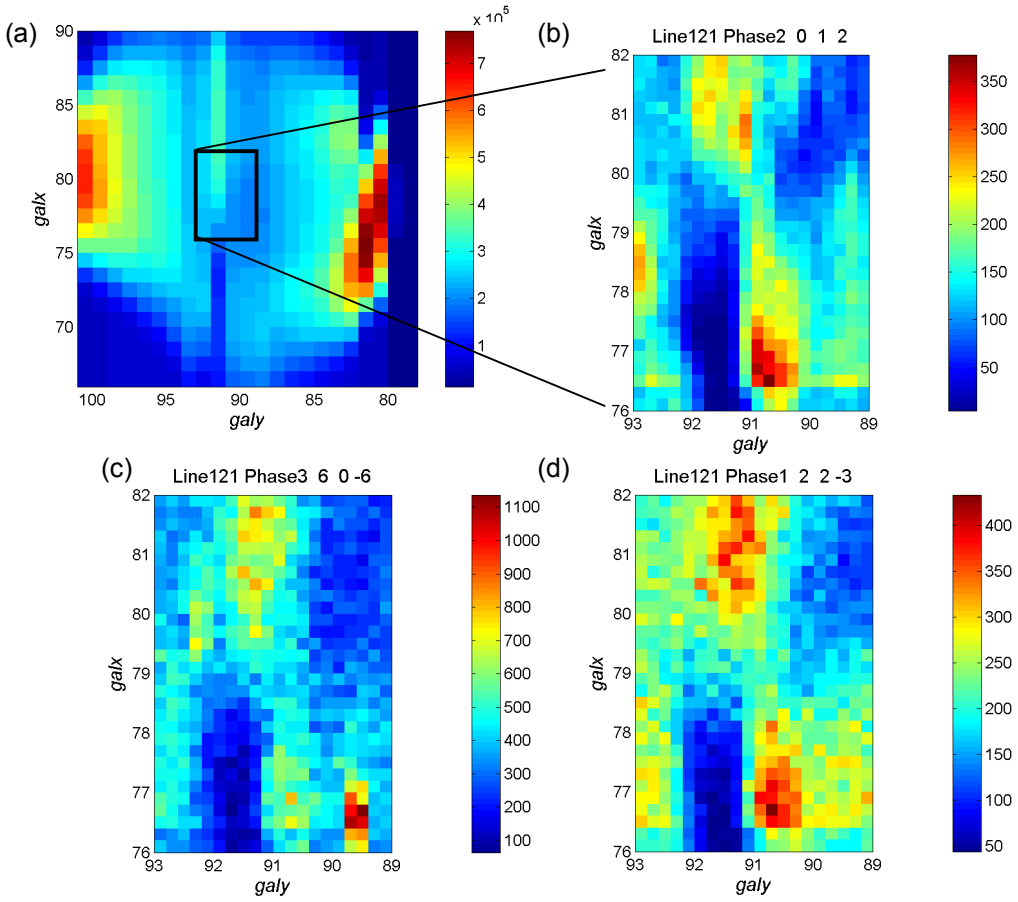

Figure 9: (a) distribution of total diffracted intensity overlaid with a box indicating the fine scan region and intensity distributions of (b) portlandite 0 1 2 reflection (recorded at 49.1 keV), (c) C_2S 2 2 $\bar{3}$ reflection (recorded at 51.8 keV), (d) CSH 6 0 $\bar{6}$ recorded at 43.1 keV. These plots are derived from data recorded at position *galz* = 121.

4 Discussion

The pre-carbonated hydrated white cement samples, which had little or no exposure to air, showed no evidence of carbonation. SEM and XRD demonstrated that the samples exposed to the 2hr accelerated carbonation showed evidence of calcite formation only on the surface of the major fracture. Such material was not detectable in the TEDDI data, even in the medium resolution scan. This signifies that the depth of carbonation at the fracture surface was considerably less than 200 um and consequently was too shallow for detection by TEDDI; experience with TEDDI has indicated a realistic detection limit of about 1% by weight. The Bragg reflection intensity distribution plots presented indicate the distribution of identified crystalline phases present in the treated hydrated white cement core. However, these need to be corrected for incident beam intensity changes, and most importantly for changes in X-ray path length. This is the first study where 3D *TEDDI* has been employed, though we essentially report insignificant carbonate concentrations after just 2 hours of simulated carbonation. However the method offers real promise for conducting long term non-destructive time-line studies when significant solid-state changes are expected; such a study, of natural versus simulated carbonation within concrete, will be ongoing during 2006 and 2007.

5 References

[1] C. Hall, P. Barnes, J.K. Cockcroft, S.L. Colston, D. Hausermann, S.D.M Jacques, A.C. Jupe, M. Kunz, Synchrotron energy-dispersive x-ray diffraction tomography, Nucl Instr Meth Phys Res B 140 (1998) 253-257

[2] P. Barnes, A.C. Jupe, S.D.M. Jacques, S.L. Colston, J.K. Cockcroft, D. Hooper, M. Betson, C. Hall, S. Barè, A.R. Rennie, J. Shannahan, M.A. Carter, W.D. Hoff, M.A. Wilson, M.C. Phillipson, Tomographic energy-dispersive diffraction imaging of static and dynamic systems, Non-destr Test Eval 17 (2001) 143-167

[3] C. Hall, S.L. Colston, A.C. Jupe, S.D.M. Jacques, R. Livingston, E.S. Ramdan, P. Barnes, Non-destructive energy-dispersive diffraction imaging of the interior of bulk concrete, Cem Concr Res 30 (2000) 491-495

[4] A.P. Wilkinson, C. Lind, S.R. Stock, K.E. Kurtis, N.Naik, D.R. Haeffner, P.L. Lee, Mapping the distribution of corrosion products in cement exposed to sulfate using energy dispersive X-ray diffraction, Mat Res Soc Symp Proc MRS (2001) 678

[5] G J Verbeck, Carbonation of hydrated Portland cement, Research and development Bulletin, Portland Cement Association, 1958

[6] Sarott F.-A. ; Bradbury M. H. ; Pandolfo P, Spieler P, Diffusion and adsorption studies on hardened cement paste and the effect of carbonation on diffusion rates, Cem Concr Res, 22 (1992) 439-444

[7] P. J. Dewaele; E. J. Reardon; R. Dayal, Permeability and porosity changes associated with cement grout carbonation Cem Concr Res 21 (1991) 441-54.

[8] M. Betson, J. Barker, P. Barnes, T. Atkinson, A. Jupe, Porosity imaging in porous media using synchrotron tomographic techniques, Transport in Porous Media 57 (2004) 203

[9] S.M. Clark, A new energy-dispersive powder diffraction facility at the SRS, Nucl Instr Meth Phys Res A 381 (1996), 161-168

[10] P. Barnes, A. C. Jupe, S. L. Colston, S. D. M Jacques, A. Grant, T. Rathbone; M Miller.; S M Clark, R. J. Cernik, A New Three-Angle Energy-Dispersive Diffractometer. Nucl Instr Meth Phys Res B 134 (1998) 310-313

[11] A. LeBail, D.Louer, Direct determination of fourier coefficients in x-ray line-pro/file analysis, Bulletin de la societe Francaise Mineralogie et de Cristallographie 99 (4) (1976) 211-215

[12] B. Hunter, Rietica- A visual Rietveld program, IUCr Powder Diffraction 20 (1998) 21

[13] http://www.rietica.org/

[14] W.G. Mumme, R.J. Hill, G.W. Bushnell, E.R. Segnit, Rietveld crystal-structure refinements, crystal-chemistry and calculated powder diffraction data for the polymorphs of dicalcium silicate and related phases Neues Jahrbuch fuer Mineralogie. Abhandlungen 169 (1995) 35-68

[15] T. Nagai, T. Ito, T. Hattori, T. Yamanaka, Compression mechanism and amorphization of portlandite, Ca(OH)(2): structural refinement under pressure Phys & Chem Miner 27 (2000) 462-466

[16] H. Taylor; Univeristy of Aberdeen, ICDD grant in aid (1980).

[17] T. Pilati, F. Demartin, C.M. Gramaccioli, Lattice-dynamical estimation of atomic displacement parameters in carbonates: Calcite and aragonite CaCO3, dolomite CaMg(CO3)(2) and magnesite MgCO3 Acta Cryst 54 B (1998) 515-523